# Supporting Information

## Synthesis Route Effects on Structure and Electrochemical Performance of Layered Oxide Cathode for Na-ion Batteries

Arnob Dey, [a] Sharmin Akter,[a] Arjun Thapa,[b] Jacek B. Jasinski,[b] Hui Wang [a] *

a. Mechanical Engineering Department, University of Louisville, Louisville, KY, 40292

b. Conn Center for Renewable Energy Research, University of Louisville, Louisville, KY, 40292

Corresponding author: hui.wang.1@louisville.edu

**Experimental Section**

**1.1 Material Synthesis**

Layered oxide $Na_{0.67}Fe_{0.5}Mn_{0.5}O_2$ cathode material was synthesized using both co-precipitation and solid-state synthesis method. For co-precipitation synthesis the primary material $Fe_{0.5}Mn_{0.5}CO_3$ was produced mixing $FeSO_4$, $MnSO_4$ (1:1 ratio) 1M solution in 100ml deionized water and 100 ml $Na_2CO_3$ 1M solution with a continuous magnetic stir. The $CO_2$ gas was supplied continuously. Then the material was calcinated using $Na_2CO_3$ with $Fe_{0.5}Mn_{0.5}CO_3$ in stochiometric ratio. 5% excess of $Na_2CO_3$ was used to compensate the Na loss.

For the solid-state synthesis, the precursors $Na_2CO_3$, $Fe_2O_3$ and $MnO_2$ was mixed in stochiometric ratio and the ball milling process was carried out for 2h using zirconia balls. Two step heat treatment process was carried out during calcination process. Initially, the mixture was heated to 450℃ at 5℃ per min and annealed for 5h reducing the temperature to room temperature after annealing. The mixture was mixed again with mortar pestle to reduce the carbonate formation on the substrate and again annealed at 850℃ for 12h with a ramp rate of 5℃ per min. After cooling down to room temperature the material immediately transferred to the Ar-filled glovebox.

**1.2 Structural Characterization**

The powder samples during synthesis process were subjected to structural characterization by X-ray diffraction using a Bruker D8 Discover diffractometer (nickel-filtered Cu Kα radiation, λ = 1.5418 Å) in a 2θ range of 10-70◦. The morphology and structure of the samples were characterized by a scanning electron microscope (SEM, TESCAN Vega3). TEM analysis was performed using Talos F200 and Tecnai F20 electron microscopes (Thermo Fisher Scientific).

**1.3 Electrochemical Characterization**

CR2032 coin cells were assembled with NFMO as active material in cathode, Na foil as anode, and glass fiber separator. The produced $Na_{0.67}Fe_{0.5}Mn_{0.5}O_2$ material was used to prepare composite cathode through dry processing approach in ambient environment. Specifically, the NFMO powder (5 mg) was mixed with TAB-2 binder (3 mg) in a mortar pestle to obtain a homogeneous mixture that load on a stainless-steel mesh, followed by drying at 170 ℃ for 3h. The liquid electrolyte is 1M $NaPF_6$ solution in EC/DEC solvent (1:2) with 5 vol% of fluoroethylene

carbonate (FEC) as additive. The galvanostatic discharge-charge of the coin cells are performed in the voltage range of 2.0–4.3 V at 30 °C. The electrochemical cycling data measured on the electrochemical the NeWare battery testing system. 1C is defined as fully charging the cathode in 1 hour, which corresponded to the current rate of 140 mA $g^{-1}$. The dQ/dV curve obtained from the charge-discharge profile of both the cathodes. The rate of performance is compared for both SS-NFMO and CP-NFMO at 0.2 C, 0.5 C, 1 C, 2 C and resume to 0.1 C rate.

### 1.4 GITT Experiment

The diffusion coefficient (D) of $Na^+/Na$ was determined via galvanostatic intermittent titration technique (GITT). The GITT measurement was done in Neware battery testing system. Here, the voltage response was measured after applying a fixed current pulse for 30 mins followed by a resting period of 2h which allowed the electrode to reach a steady-state of voltage. The diffusion coefficient (D) was calculated using the following equation-

$$D = \frac{4}{\pi\tau}\left(\frac{m_B V_M}{M_B S}\right)^2 \left(\frac{\Delta E_s}{\Delta E_\tau}\right)^2$$

where, $\tau$ is the pulse duration, $m_B$ and $M_B$ are active mass and molecular weight of NFMO. In addition, S represents the active surface area of NFMO cathode. The molar volume ($V_M$) based on the molar density ($\rho = 4.09 \times 10^3\ kg\ m^{-3}$) and then calculated for $Na_{0.67}Fe_{0.5}Mn_{0.5}O_2$ as $25.13\ cm^3\ mol^{-1}$. The voltage response $\Delta E_s$ and $\Delta E_\tau$ were obtained from the GITT curve.

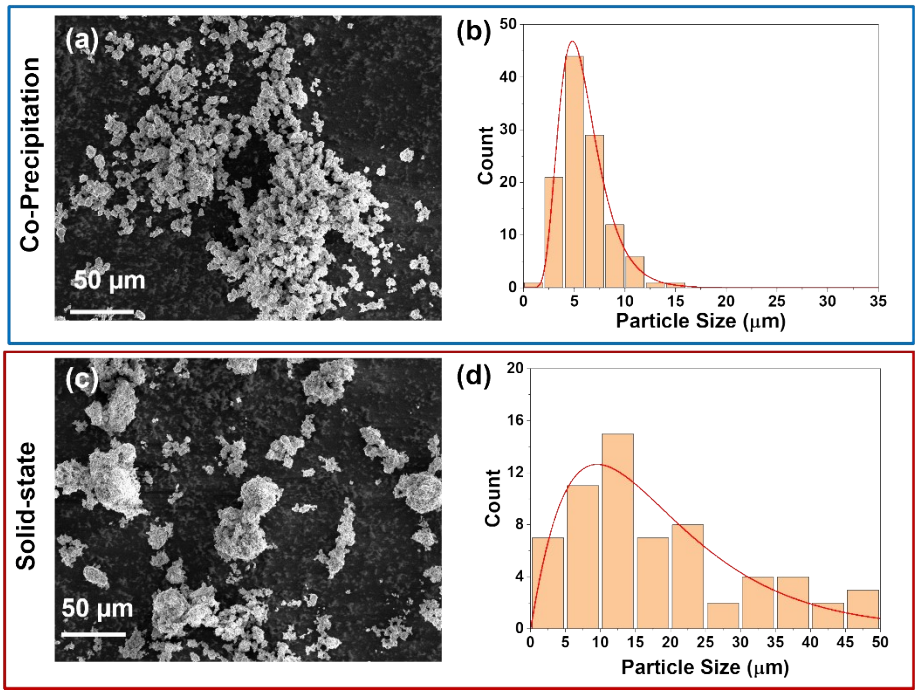


Figure S1: SEM images and particle size statistics analysis of secondary particles in: (a) (b) Co-precipitation, (c) (d) Solid-state

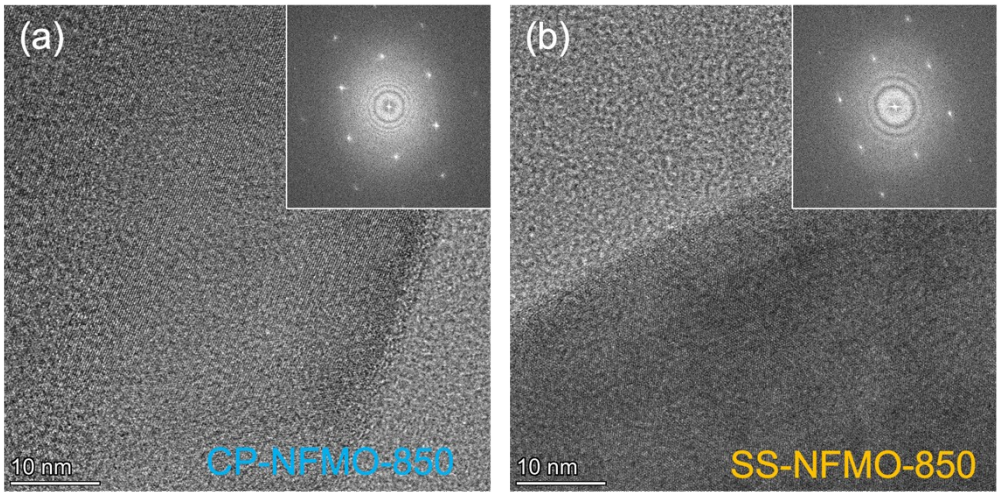


Figure S2: Plane-view HRTEM images and corresponding FFT patterns of (a) CP-NFMO-850, and (b) SS-NFMO-850 samples.

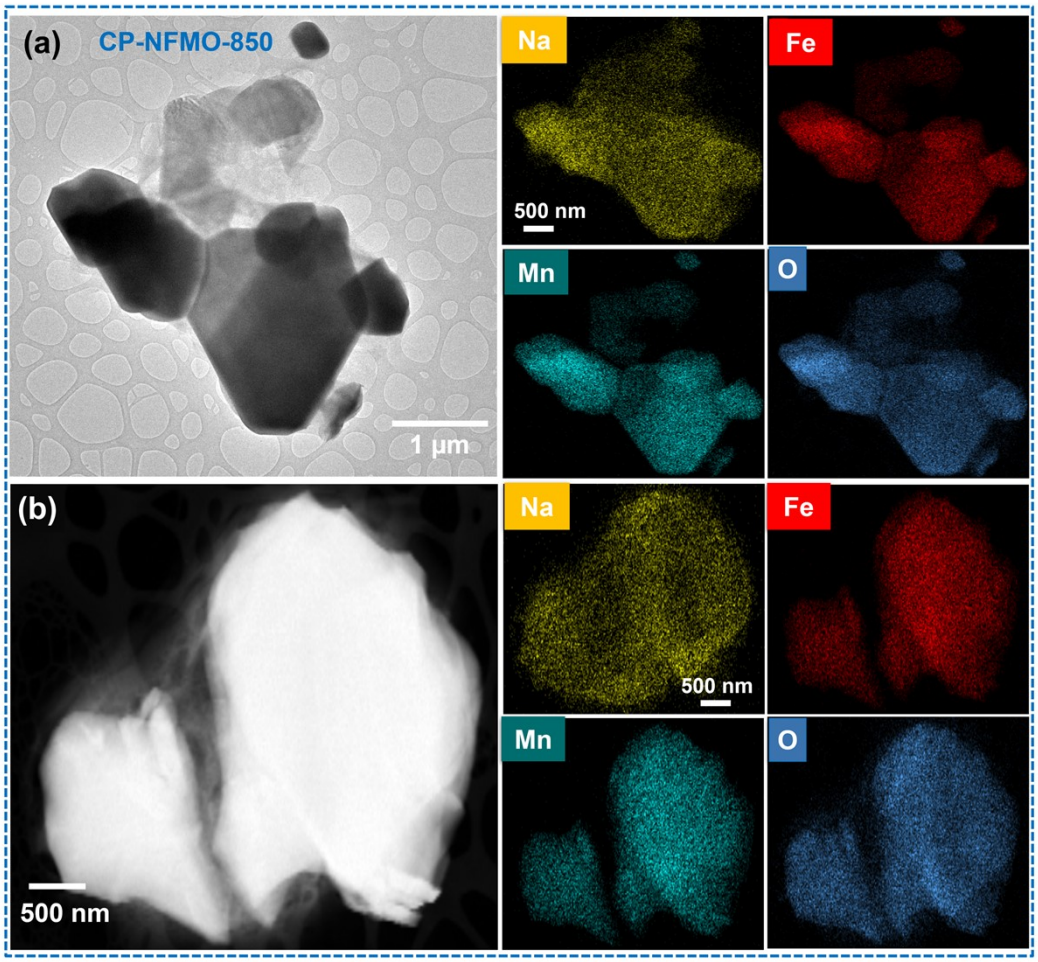


Figure S3: CP-NFMO-850 sample: TEM/STEM images and corresponding EDS-based elemental maps from (a) Region I; (b) Region II.

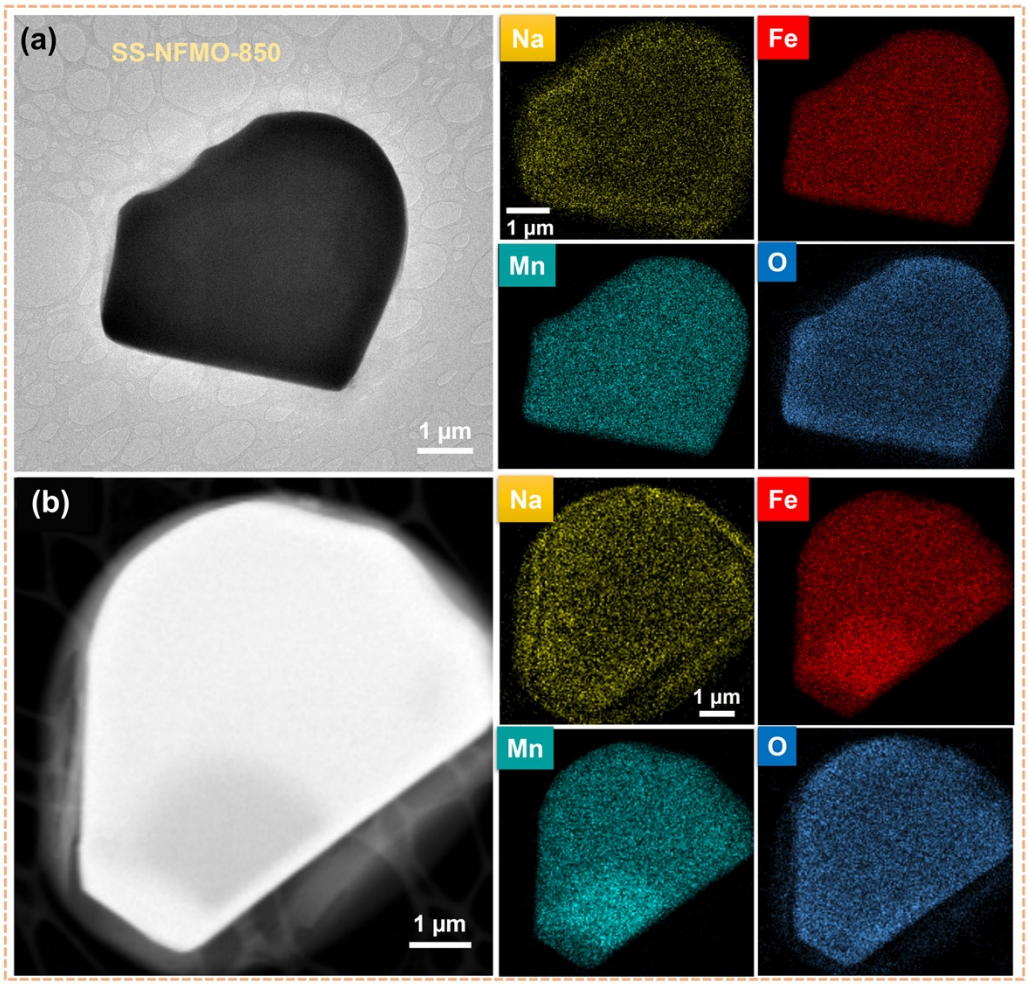


Figure S4: SS-NFMO-850 sample: TEM/STEM images and corresponding EDS-based elemental maps from (a) Region I; (b) Region II.

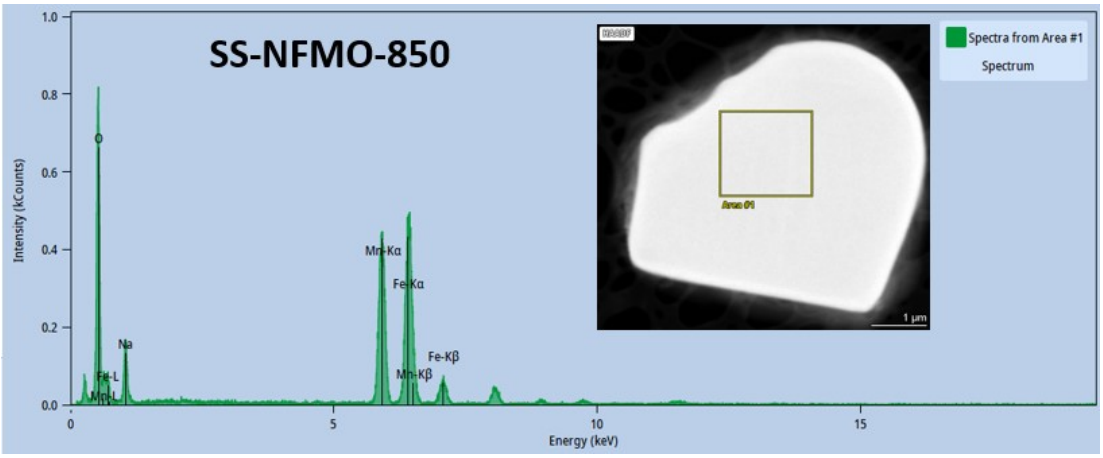


| Z | Element | Family | Atomic Fraction (%) | Atomic Error (%) | Mass Fraction (%) | Mass Error (%) |
|---|---|---|---|---|---|---|
| 8 | O | K | 50.19 | 2.31 | 24.09 | 1.77 |
| 11 | Na | K | 7.07 | 1.35 | 4.88 | 0.99 |
| 25 | Mn | K | 20.91 | 2.67 | 34.46 | 3.92 |
| 26 | Fe | K | 21.83 | 2.40 | 36.58 | 3.68 |

Figure S5. SS-NFMO-850 sample: high-angle annular dark-field (HAADF)-STEM image and the corresponding spectrum for the area 1 from HR-TEM.

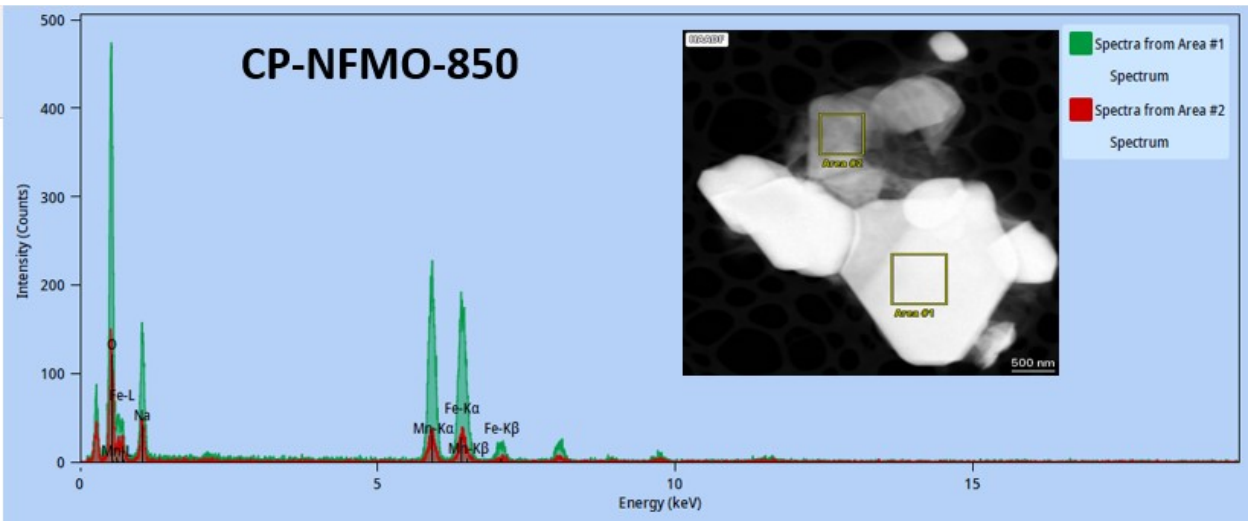


| Z-area 1 | Element | Family | Atomic Fraction (%) | Atomic Error (%) | Mass Fraction (%) | Mass Error (%) |
|---|---|---|---|---|---|---|
| 8 | O | K | 55.80 | 2.33 | 30.38 | 2.00 |
| 11 | Na | K | 12.38 | 2.21 | 9.69 | 1.85 |
| 25 | Mn | K | 17.38 | 2.32 | 32.50 | 3.69 |
| 26 | Fe | K | 14.44 | 1.73 | 27.43 | 3.04 |
| **Z-area 2** | **Element** | **Family** | **Atomic Fraction (%)** | **Atomic Error (%)** | **Mass Fraction (%)** | **Mass Error (%)** |
| 8 | O | K | 64.71 | 2.41 | 41.48 | 2.26 |
| 11 | Na | K | 15.22 | 2.61 | 14.02 | 2.50 |
| 25 | Mn | K | 10.33 | 1.49 | 22.73 | 2.90 |
| 26 | Fe | K | 9.77 | 1.22 | 21.77 | 2.48 |

Figure S6. CF-NFMO-850: HAADF-STEM image and the corresponding spectrum for two selected areas.

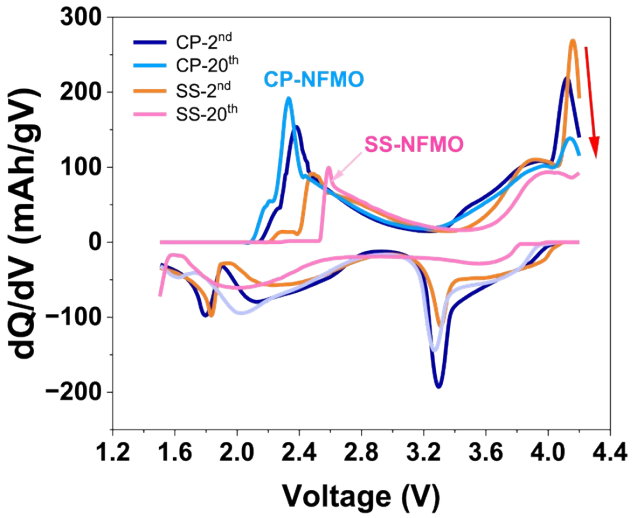


Figure S7: dQ/dV curve of CP-NFMO and SS-NFMO samples ($2^{nd}$, $20^{th}$ cycles)

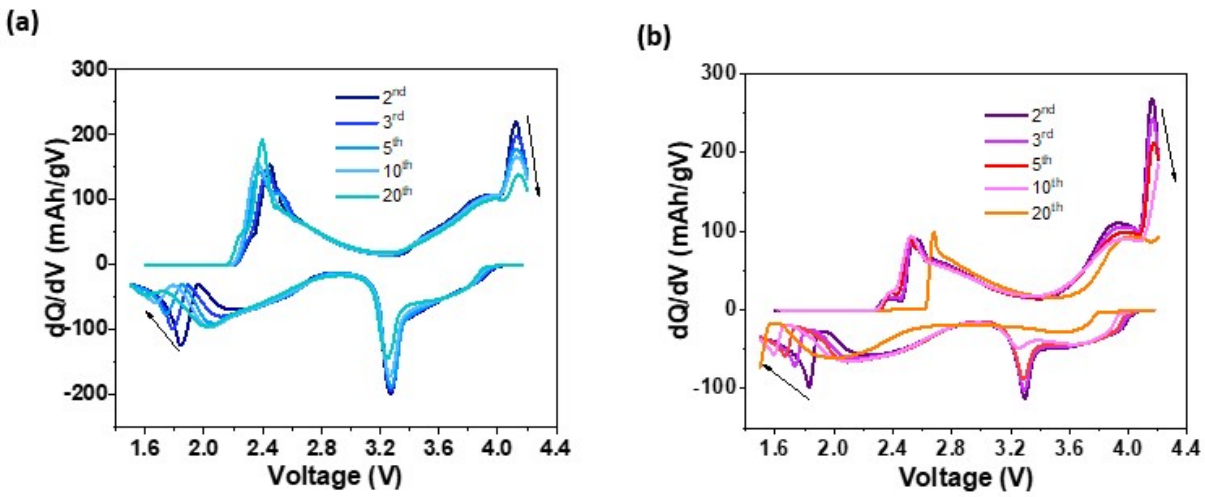


Figure S8: dQ/dV curves of (a) CP-NFMO and (b) SS-NFMO sample ($2^{nd}$, $3^{rd}$, $5^{th}$, $10^{th}$, $20^{th}$ cycles).

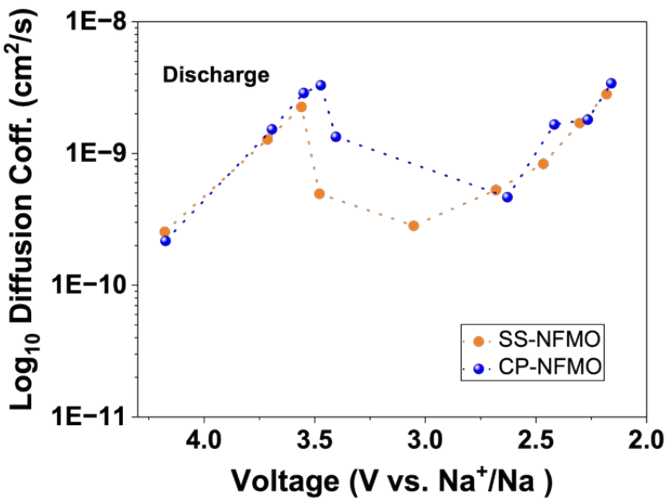


Figure S9: Diffusion coefficient comparison between SS-NFMO and CP-NFMO for discharge process.

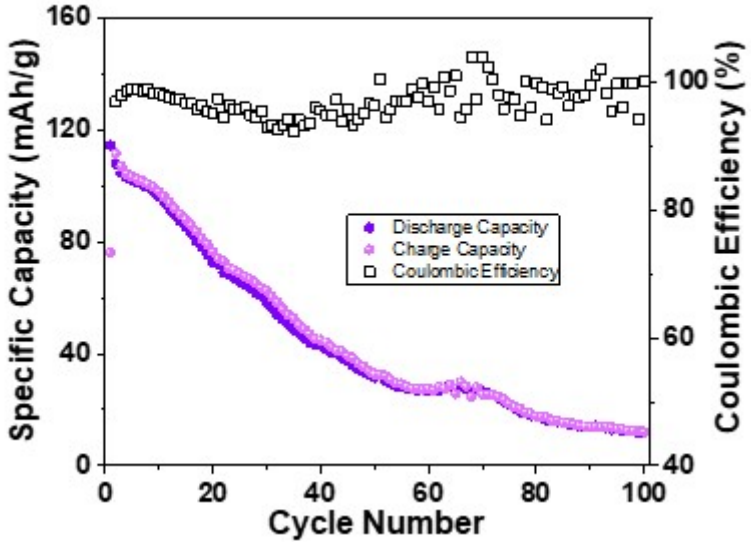


Figure S10: Electrochemical cycling of SS-NFMO for 100 cycles at 1C (140 mAh as 1C).

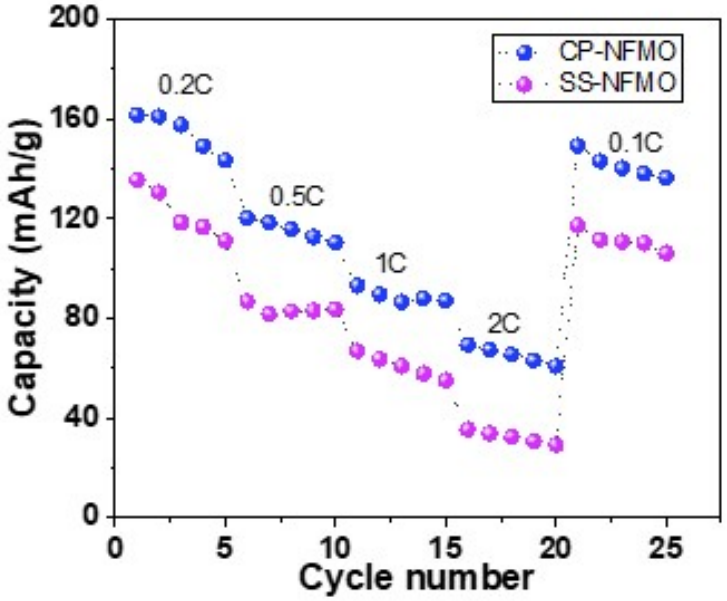


Figure S11: Electrochemical rate capacity comparison between CP-NFMO and SS-NFMO.

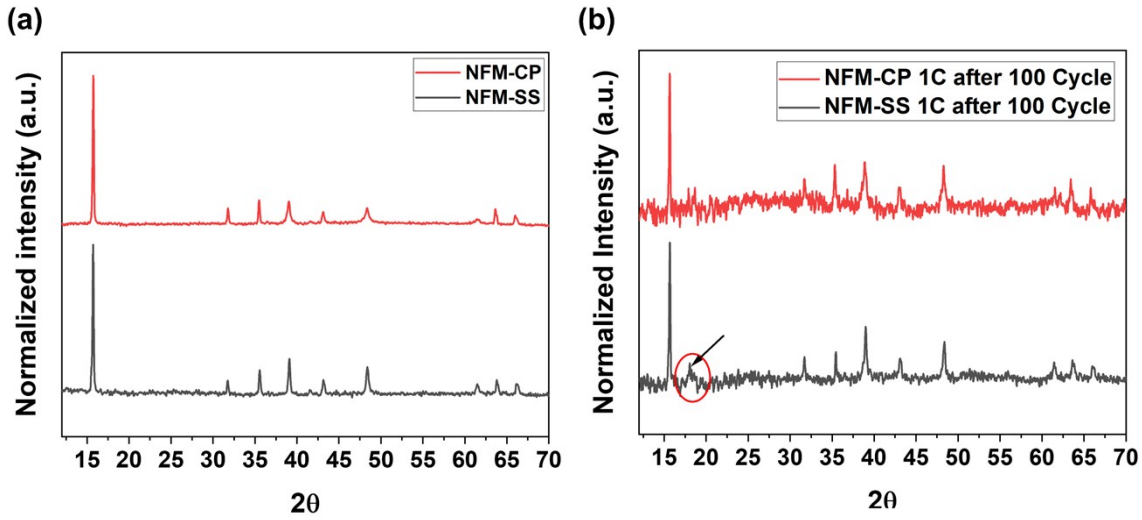


Figure S12: Ex-situ XRD patterns of CP-NFMO and SS-NFMO (a) pristine samples (b) after 100 cycles at 1C.

Table S1. XRD Rietveld refinement results for CP-NFMO-850 and SS-NFMO-850 samples.

| **Sample: CP-NFMO-850** | | | | Lattice Parameters: a= 2.921 Å, b=2.53 Å, c=11.258 Å | | | |
|---|---|---|---|---|---|---|---|
| **h** | **k** | **l** | **d-spacing** | **2-theta** | **F_obs** | **F_calc** | **FWHM** |
| 0 | 0 | 2 | 5.6292 | 15.72918 | 3083.179 | 2573.226 | 0.12775 |
| 0 | 0 | 4 | 2.8146 | 31.76491 | 2423.826 | 1783.783 | 0.21583 |
| 1 | 0 | 0 | 2.5299 | 35.45092 | 1207.719 | 966.741 | 0.23803 |
| 1 | 0 | 1 | 2.4684 | 36.36548 | 61.059 | 46.165 | 0.24364 |
| 1 | 0 | 2 | 2.3076 | 38.99813 | 759.172 | 482.229 | 0.26005 |
| 1 | 0 | 3 | 2.0978 | 43.08352 | 576.78 | 393.814 | 0.28625 |
| 1 | 0 | 4 | 1.8816 | 48.33087 | 1915.777 | 1608.091 | 0.3213 |
| 0 | 0 | 6 | 1.8764 | 48.47212 | 64.489 | 52.921 | 0.32226 |
| 1 | 0 | 5 | 1.682 | 54.50907 | 199.733 | 74.667 | 0.36481 |
| 1 | 0 | 6 | 1.5071 | 61.47142 | 1088.461 | 845.754 | 0.4172 |
| 1 | 1 | 0 | 1.4607 | 63.65098 | 2958.56 | 2299.685 | 0.43443 |
| 1 | 1 | 2 | 1.4138 | 66.02162 | 1057.546 | 702.669 | 0.45368 |
| 0 | 0 | 8 | 1.4073 | 66.36798 | 647.632 | 503.686 | 0.45653 |
| 1 | 0 | 7 | 1.3573 | 69.15157 | 8.104 | 0.794 | 0.47994 |

| **Sample: SS-NFMO-850** | | | | Lattice Parameters: a=2.915Å, b=2.525Å, c=11.274Å | | | |
|---|---|---|---|---|---|---|---|
| **h** | **k** | **l** | **d-spacing** | **2-theta** | **F_obs** | **F_calc** | **FWHM** |
| 0 | 0 | 2 | 5.63742 | 15.70607 | 3661.413 | 2574.264 | 0.1325 |
| 0 | 0 | 4 | 2.81871 | 31.71732 | 3368.899 | 1784.971 | 0.16279 |
| 1 | 0 | 0 | 2.52454 | 35.52923 | 1309.906 | 966.016 | 0.17081 |
| 1 | 0 | 1 | 2.46354 | 36.43946 | 58.081 | 45.989 | 0.17278 |
| 1 | 0 | 2 | 2.30406 | 39.06039 | 958.563 | 481.892 | 0.17856 |
| 1 | 0 | 3 | 2.09564 | 43.12944 | 686.438 | 393.063 | 0.18788 |
| 1 | 0 | 4 | 1.88055 | 48.35822 | 2267.236 | 1607.051 | 0.20055 |
| 0 | 0 | 6 | 1.87914 | 48.39684 | 75.091 | 52.832 | 0.20065 |
| 1 | 0 | 5 | 1.68176 | 54.51687 | 326.896 | 74.641 | 0.21657 |
| 1 | 0 | 6 | 1.50739 | 61.45906 | 1495.301 | 846.022 | 0.23628 |
| 1 | 1 | 0 | 1.45754 | 63.80308 | 3329.105 | 2289.98 | 0.24337 |
| 1 | 1 | 2 | 1.41114 | 66.16397 | 1369.724 | 700.133 | 0.25077 |
| 0 | 0 | 8 | 1.40935 | 66.25863 | 1017.706 | 504.652 | 0.25107 |
| 1 | 0 | 7 | 1.35786 | 69.11818 | 18.477 | 0.795 | 0.2604 |

Table S2. Comparison of synthesis methods, crystal structure and capacity for NFMO cathode.

| Cathode composition | Synthesis method | Structure | Voltage/ rate | Heating temp/time | Initial Capacity (mAh/ g) | Retention (cycles) | Ref |
|---|---|---|---|---|---|---|---|
| $Na_{0.67}Fe_{0.5}Mn_{0.5}O_2$ | Solid-state | P-2 | 1.5-4.3V/ 0.1C | 900℃/12h, | 179.3 | 54.6% (100) | 1 |
| $Na_{0.67}Fe_{0.5}Mn_{0.5}O_2$ | Sol-gel | P-2 | 1.5-4.0V/ 0.1C | 900℃/12h, | 166.1 | 73.64% (100) | 2 |
| $Na_{0.67}Fe_{0.5}Mn_{0.5}O_2$ | Sol-gel | P-2 | 1.5-4.3V/ 0.1C | 900℃/ 12h | 147.8 | 63.3% (50) | 3 |
| $Na_{0.67}Fe_{0.5}Mn_{0.5}O_2$ | Solution combustion | P-2 | 1.5-4.3V/ 0.1C | 900℃/ 6h | 166 | 67% (100) | 4 |
| $Na_{0.67}Fe_{0.5}Mn_{0.5}O_2$ | Solid-state | P-2 | 1.5-4.2V/ 0.1C | 1000℃/12h | 151 | 81% (15) | 5 |
| $Na_{0.67}Fe_{0.5}Mn_{0.5}O_2$ | Sol-gel | P-2 | 1.5-4.3V/ 0.1C | 900℃ /15h | 177.5 | 52% (40) | 6 |
| $Na_{0.67}Fe_{0.5}Mn_{0.5}O_2$ | Self-combustion | P2 | 1.5-4.2V/ 0.1C | 1000℃/6h | 210 | 50% (40) | 7 |
| $Na_{0.67}Fe_{0.5}Mn_{0.5}O_2$ | Solid-state | P-2 | 1.5-4.5V/ 10mA/g | 950℃/10h | 178 | 79.8% (100) | 8 |
| $Na_{0.67}Fe_{0.5}Mn_{0.5}O_2$ | Sol-gel | P-2 | 2.0-4.0V/ 1C | 900℃/12h | 164.3 | 54.6% (200) | 9 |
| $Na_{0.67}Fe_{0.5}Mn_{0.5}O_2$ | Hydro-thermal | P-2 | 1.5-4.5V/ 200mA/g | 850℃/11h | 137 | 73% (50) | 10 |
| $Na_{0.67}Fe_{0.5}Mn_{0.5}O_2$ | **Co-precipitation** | **P-2** | **1.5-4.2V/ 1C** | **850℃ /12h** | **135** | **60% (100)** | **This work** |

## Reference


1. L. Qian, R. Huang, H. Zhang, S. Yan and S. Luo, *ACS Applied Energy Materials*, 2024, **7**, 8136-8146.
2. H. Xue, S. Liu, Y. Liu, H. Qiu, J. Cui, Q. Liu, Y. Zhang and W. He, *Journal of Colloid and Interface Science*, 2025, **685**, 87-96.
3. Z. Li, W. Kong, Y. Yu, J. Zhang, D. Wong, Z. Xu, Z. Chen, C. Schulz, M. Bartkowiak and X. Liu, *Angewandte Chemie*, 2022, **134**.
4. V. K. Kumar, S. Ghosh, S. Biswas and S. K. Martha, *Journal of The Electrochemical Society*, 2021, **168**, 030512.

5. E. Gonzalo, M. H. Han, J. M. López Del Amo, B. Acebedo, M. Casas-Cabanas and T. Rojo, *J. Mater. Chem. A*, 2014, **2**, 18523-18530.
6. Y. Bai, L. Zhao, C. Wu, H. Li, Y. Li and F. Wu, *ACS Applied Materials & Interfaces*, 2016, **8**, 2857-2865.
7. R. Viswanatha, B. Kishore, U. Bharath and N. Munichandraiah, *Journal of The Electrochemical Society*, 2018, **165**, A263-A265.
8. E. Boivin, R. A. House, J. J. Marie and P. G. Bruce, *Advanced Energy Materials*, 2022, **12**, 2200702.
9. G. Zhang, J. Li, Y. Fan, Y. Liu, P. Zhang, X. Shi, J. Ma, R. Zhang and Y. Huang, *Energy Storage Materials*, 2022, **51**, 559-567.
10. X. Zhou, X. Huang, Y. Cui, Y. Zhu, L. Wang, X. Wang and S. Tang, *ACS Applied Materials & Interfaces*, 2024, **16**, 36354-36362.